Supporting Information (the part 01) for:

Theoretical study on the catalytic mechanism of the retaining α-1,2-mannosyltransferase Kre2p/Mnt1p: The impact of diferent metal ions on catalysis

Adela Bobovská,[a,b] *Igor Tvaroška,*[a] *Juraj Kóňa*[a*]

[a] Institute of Chemistry, Center for Glycomics, Slovak Academy of Sciences, Dúbravska cesta 9, 845 38 Bratislava, Slovak Republic
[b] Comenius University, Faculty of Natural Sciences, Department of Physical and Theoretical Chemistry, Mlynská Dolina CH-1, 842 15 Bratislava 4, Slovak Republic

E-mail: chemkona@savba.sk

Contents:

Table S1. Docking scores (Glide SP) (in kcal mol^{-1}), selected interatomic distances (d) (in Å), valence (φ) and torsion angles (ϕ) (in degrees) for twenty poses of a mannosyl cation docked into the active site of Kre2p in presence of the bound donor (GDP) and acceptor (methyl-α-mannoside) moieties. For atom numbering see Figure 2.

Table S2. Selected geometry parameters, interatomic distances (d) (in Å), of the optimized transition states and intermediates for the wild-type enzyme with the Mg^{2+} cofactor (**WT_Mg**) calculated at the hybrid DFT-M06-2X:OPLS2005 and DFT-B3LYP:OPLS2005 levels. For atom numbering see Figure 2.

Table S3. Selected geometry parameters, interatomic distances (d) (in Å), of the optimized transition states and intermediates for the wild-type enzyme with the Zn^{2+} cofactor (**WT_Zn**) calculated at the hybrid DFT-M06-2X:OPLS2005 and DFT-B3LYP:OPLS2005 levels. For atom numbering see Figure 2

Table S4. Selected geometry parameters, interatomic distances (d) (in Å), of the optimized transition states and intermediates for the wild-type enzyme with the Ca^{2+} cofactor (**WT_Ca**) calculated at the hybrid DFT-M06-2X:OPLS2005 and DFT-B3LYP:OPLS2005 levels. For atom numbering see Figure 2

Table S5. Selected geometry parameters, valence (φ) and torsion angles (ϕ) (in degrees) of the optimized transition states and intermediates for the wild-type enzyme with the Mn^{2+} ion (**WT_Mn**) calculated at the hybrid DFT-M06-2X:OPLS2005 and DFT-B3LYP:OPLS2005 levels. For atom numbering see Figure 2.

Table S6. Selected geometry parameters, valence (φ) and torsion angles (ϕ) (in degrees) of the optimized transition states and intermediates for the wild-type enzyme with the Mg^{2+} ion (**WT_Mg**) calculated at the hybrid DFT-M06-2X:OPLS2005 and DFT-B3LYP:OPLS2005 levels. For atom numbering see Figure 2.

Table S7. Selected geometry parameters, valence (φ) and torsion angles (ϕ) (in degrees) of the optimized transition states and intermediates for the wild-type enzyme with the Zn^{2+} ion (**WT_Zn**) calculated at the hybrid DFT-M06-2X:OPLS2005 and DFT-B3LYP:OPLS2005 levels. For atom numbering see Figure 2.

Table S8. Selected geometry parameters, valence (φ) and torsion angles (ϕ) (in degrees) of the optimized transition states and intermediates for the wild-type enzyme with the Ca^{2+} ion (**WT_Ca**) calculated at the hybrid DFT-M06-2X:OPLS2005 and DFT-B3LYP:OPLS2005 levels. For atom numbering see Figure 2.

Table S9. Conformations of the mannose ring of the donor substrate according to the Cremer-Pople parameters and ring puckering geometrical parameters (φ, θ, Q) calculated for the DFT-M06-2X:OPLS2005 and DFT-B3LYP:OPLS2005 optimized transition states and intermediates of the wild-type enzyme with the Mn^{2+}, Mg^{2+}, Zn^{2+} and Ca^{2+} ions (**WT_Mn**, **WT_Mg, WT_Zn** and **WT_Ca**).

Table S10. Total electronic energies ($E_{QM:MM}$) for the optimized transition states and intermediates for the wild-type enzyme with the Mn^{2+} (**WT_Mn**), Mg^{2+} (**WT_Mg**), Zn^{2+} (**WT_Zn**) and Ca^{2+}(**WT_Ca**) ions calculated at the hybrid DFT-M06-2X:OPLS2005 and DFT-B3LYP:OPLS2005 levels (in a.u.).

Table S11. Calculated pK_a values for selected ionizable amino acid residues in the active site of Kre2p, which are in direct contact with either the Mn^{2+} ion, GDP-Man^{2-} or Met-Man, for six enzyme states.

Computational details and results for pK_a and docking calculations

Figure S1. (a) Mannosyl cation (in blue) docked into the active site of Kre2p (10 poses with the best docking score) bound to the A and B binding sites (see also Table S1). (b) The docked pose no A1 [ϕ($P1_D$-$O1_D$-$C1_D$-$O5_D$) = 168.5°] with selected geometry parameters (dist ances in Å).

Figure S2. An overlay of the optimized oxocarbenium ion (**2B**, **WT_Mn**, in green**)** with the crystal structure (in orange) of Kre2p (1S4P).

Table S1. Docking scores (Glide SP) (in kcal mol^{-1}), selected interatomic distances (d) (in Å), valence (φ) and torsion angles (ϕ) (in degrees) for twenty poses of a mannosyl cation docked into the active site of Kre2p in presence of the bound donor (GDP) and acceptor (methyl-α-mannoside) moieties. For atom numbering see Figure 2.

Pose No.	Glide SP	Binding site[a]	$C1_D$-$O2_A$[b]	d($O1_D$-$C1_D$)	d($C1_D$-$O2_A$)	d(O_{Tyr220}-$O2_A$)	φ($O1_D$-$C1_D$-$O5_D$)	φ($O2_A$-$C1_D$-$O5_D$)	ϕ($P1_D$-$O1_D$-$C1_D$-$O5_D$)
1	-7.49	A	α-face	4.210	3.166	4.691	37.4	38.4	168.5
2	-7.37	A	β-face	4.994	3.529	3.731	29.0	48.1	0.8
3	-7.16	A	α-face	5.116	3.572	5.203	27.7	43.7	–148.4
4	-6.87	A	α-face	5.495	3.662	5.279	28.1	43.5	–151.8
5	-6.79	B	β-face	8.055	9.790	10.051	12.2	124.4	–31.8
6	-6.50	B	β-face	6.876	8.353	9.053	15.9	126.0	36.9
7	-6.41	B	β-face	6.914	8.483	9.029	15.2	127.5	29.1
8	-6.41	B	β-face	6.617	7.994	8.909	17.1	121.4	94.9
9	-6.19	B	β-face	6.715	7.978	8.753	17.5	119.4	75.7
10	-6.19	B	β-face	7.920	9.724	10.060	11.91	127.2	–16.7
11	-6.16	B	β-face	7.739	9.497	10.027	12.5	118.9	–138.2
12	-6.16	B	β-face	7.272	9.010	9.402	13.4	118.0	170.5
13	-6.11	B	β-face	7.545	9.297	9.841	12.8	118.6	–146.7
14	-6.09	B	β-face	6.436	7.832	8.457	17.4	123.2	32.9
15	-6.05	B	β-face	6.114	7.460	8.467	18.6	121.6	77.4
16	-5.96	B	β-face	6.484	7.726	8.504	18.2	119.0	76.2
17	-5.88	B	β-face	6.850	8.327	8.972	16.0	124.0	20.4
18	-5.84	B	α-face	7.862	9.659	9.944	12.1	123.8	–159.4
19	-5.84	B	β-face	7.203	8.588	9.442	15.8	120.9	19.4
20	-5.83	B	β-face	7.439	8.789	9.908	15.5	109.7	146.5

[a] Glide predicted two binding sites, A and B, for the mannosyl cation docked into the active site of Kre2p in the presence of the bound donor (GDP) and acceptor (methyl-α-mannoside) moieties. Only the binding site A is suitably positioned for the feasible enzymatic catalysis; [b] A position of the acceptor moiety in respect to the docked mannosyl cation, described by the position of the nucleophilic $O2_A$ oxygen of the acceptor on the α- or β-the face of the $C1_D$ reaction center carbon of the docked mannosyl cation.

Table S2. Selected geometry parameters, interatomic distances (*d*) (in Å), of the optimized transition states and intermediates for the wild-type enzyme with the Mg^{2+} cofactor (**WT_Mg**) calculated at the hybrid DFT-M06-2X:OPLS2005 and DFT-B3LYP:OPLS2005 levels. For atom numbering see Figure 2.

M06-2X (**WT_Mg**)	$d(O1_D\text{-}C1_D)$	$d(C1_D\text{-}O5_D)$	$d(C1_D\text{-}O2_A)$	$d(O1_D\text{-}H2_A)$	$d(O2_A\text{-}H2_A)$	$d(O1_D\text{-}P1_D)$	$d(O_{Y220}\text{-}C1_D)$	$d(O_{Y220}\text{-}H_{Y220})$	$d(H_{Y220}\text{-}O1_D)$
1A	1.463	1.365	4.169	2.529	0.970	1.614	3.497	0.974	1.856
1B	1.509	1.367	3.469	2.121	0.971	1.608	3.469	0.972	1.874
TS12	2.129	1.271	3.294	1.836	0.975	1.545	3.488	0.986	1.668
2A	2.292	1.261	3.307	1.795	0.976	1.535	3.487	0.989	1.645
TS22	3.268	1.249	3.027	1.542	0.993	1.527	4.332	0.993	1.604
2B	3.677	1.252	3.085	1.526	0.995	1.525	4.538	0.992	1.602
TS23	3.679	1.265	2.060	1.379	1.032	1.530	4.066	0.989	1.643
3A	3.397	1.364	1.473	1.044	1.360	1.571	3.881	0.974	1.789
3B	3.565	1.384	1.447	1.022	1.464	1.574	4.622	0.971	1.848
B3LYP (**WT_Mg**)									
1B	1.573	1.359	3.563	2.327	0.972	1.615	3.601	0.975	1.930
TS12	2.235	1.275	3.417	1.872	0.989	1.552	3.559	0.989	1.708
2A	2.446	1.267	3.484	1.822	0.980	1.543	3.546	0.991	1.697
TS22	3.382	1.258	3.111	1.590	0.992	1.532	4.338	0.994	1.642
2B	3.841	1.261	3.358	1.587	0.992	1.533	4.643	0.993	1.655
TS23	3.700	1.276	2.109	1.419	1.027	1.537	4.107	0.992	1.671
3A	3.479	1.367	1.479	1.040	1.395	1.584	3.942	0.976	1.847
3B	3.656	1.386	1.465	1.015	1.522	1.589	4.617	0.973	1.882

Table S3. Selected geometry parameters, interatomic distances (*d*) (in Å), of the optimized transition states and intermediates for the wild-type enzyme with the Zn^{2+} cofactor (**WT_Zn**) calculated at the hybrid DFT-M06-2X:OPLS2005 and DFT-B3LYP:OPLS2005 levels. For atom numbering see Figure 2.

M06-2X (**WT_Zn**)	$d(O1_D\text{-}C1_D)$	$d(C1_D\text{-}O5_D)$	$d(C1_D\text{-}O2_A)$	$d(O1_D\text{-}H2_A)$	$d(O2_A\text{-}H2_A)$	$d(O1_D\text{-}P1_D)$	$d(O_{Y220}\text{-}C1_D)$	$d(O_{Y220}\text{-}H_{Y220})$	$d(H_{Y220}\text{-}O1_D)$
1B	1.506	1.368	3.302	2.131	0.971	1.609	3.502	0.972	1.894
TS12	2.129	1.271	3.295	1.837	0.975	1.545	3.495	0.987	1.661
2A	2.312	1.260	3.487	1.642	0.990	1.534	3.487	0.990	1.642
TS22	3.289	1.249	3.031	1.542	0.993	1.526	4.340	0.994	1.591
2B	3.748	1.253	3.121	1.525	0.995	1.526	4.591	0.992	1.597
TS23	3.692	1.265	2.100	1.375	1.034	1.530	4.071	0.989	1.637
3A	3.408	1.365	1.472	1.045	1.361	1.572	3.893	0.974	1.788
3B	3.563	1.383	1.448	1.022	2.463	1.575	4.634	0.971	1.846
B3LYP (**WT_Zn**)									
1B	1.566	1.361	3.571	2.336	0.972	1.616	3.600	0.975	1.941
TS12	2.235	1.274	3.416	1.852	0.978	1.552	3.545	0.989	1.704
2A	2.435	1.267	3.495	1.826	0.980	1.543	3.548	0.991	1.699
TS22	3.315	1.257	3.075	1.594	0.992	1.532	4.258	0.995	1.644
2B	3.852	1.262	3.401	1.591	0.992	1.533	4.670	0.993	1.656
TS23	3.711	1.273	2.111	1.404	1.028	1.537	4.095	0.992	1.656
3A	3.493	1.369	1.493	1.038	1.405	1.587	3.972	0.976	1.849
3B	3.635	1.386	1.467	1.016	1.517	1.589	4.634	0.973	1.870

Table S4. Selected geometry parameters, interatomic distances (*d*) (in Å), of the optimized transition states and intermediates for the wild-type enzyme with the Ca^{2+} cofactor (**WT_Ca**) calculated at the hybrid DFT-M06-2X:OPLS2005 and DFT-B3LYP:OPLS2005 levels. For atom numbering see Figure 2.

M06-2X (**WT_Ca**)	$d(O1_D\text{-}C1_D)$	$d(C1_D\text{-}O5_D)$	$d(C1_D\text{-}O2_A)$	$d(O1_D\text{-}H2_A)$	$d(O2_A\text{-}H2_A)$	$d(O1_D\text{-}P1_D)$	$d(O_{Y220}\text{-}C1_D)$	$d(O_{Y220}\text{-}H_{Y220})$	$d(H_{Y220}\text{-}O1_D)$
1B	1.512	1.367	3.282	0.971	0.971	1.611	3.529	0.973	1.877
TS12	2.125	1.272	3.284	1.849	0.976	1.547	3.515	0.988	1.644
2A	2.415	1.257	3.284	1.753	0.979	1.532	3.495	0.992	1.622
TS22	3.319	1.249	3.036	1.551	0.993	1.527	4.346	0.996	1.569
2B	3.863	1.252	3.104	1.516	0.998	1.525	4.637	0.993	1.584
TS23	3.759	1.265	2.089	1.618	0.991	1.531	4.074	0.991	1.618
3A	3.484	1.367	1.467	1.037	1.395	1.578	3.941	0.973	1.789
3B	3.619	1.383	1.446	1.016	1.504	1.581	4.673	0.972	1.827
B3LYP (**WT_Ca**)									
1B	1.576	1.360	3.521	2.318	0.972	1.619	3.617	0.975	1.916
TS12	2.401	1.268	3.463	1.844	0.980	1.546	3.634	0.991	1.687
2A	2.559	1.264	3.498	1.794	0.982	1.541	3.575	0.933	1.670
TS22	3.462	1.258	3.149	1.600	0.991	1.531	4.398	0.996	1.608
2B	3.966	1.260	3.341	1.576	0.994	1.530	4.696	0.995	1.614
TS23	3.798	1.274	2.099	1.434	1.027	1.538	4.092	0.993	1.652
3A	3.572	1.371	1.468	1.029	1.445	1.593	4.053	0.976	1.818
3B	3.747	1.388	1.464	1.009	1.579	1.597	4.698	0.973	1.875

Table S5. Selected geometry parameters, valence (φ) and torsion angles (ϕ) (in degrees) of the optimized transition states and intermediates for the wild-type enzyme with the Mn^{2+} ion (**WT_Mn**) calculated at the hybrid DFT-M06-2X:OPLS2005 and DFT-B3LYP:OPLS2005 levels. For atom numbering see Figure 2.

M06-2X (**WT_Mn**)	φ($O1_D$-$C1_D$-$O5_D$)	φ($O2_A$-$C1_D$-$O5_D$)	φ($O2_A$-$H2_A$-$O1_D$)	φ(O_{Tyr220}-H_{Tyr220}-$O1_D$)	φ(O_{Tyr220}-$C1_D$-$O5_D$)	ϕ($P1_D$-$O1_D$-$C1_D$-$O5_D$)	ϕ($O5_A$-$C2_A$-$C1_D$-$O5_D$)
1A	110.3	95.6	109.6	162.9	140.2	69.2	–37.4
1B	107.4	74.6	140.1	159.4	66.0	161.6	54.4
TS12	105.3	75.6	150.1	162.0	68.1	168.3	56.7
2A	104.7	67.9	153.2	163.0	67.9	170.4	58.1
TS22	96.0	67.2	174.9	164.7	67.2	161.0	63.7
2B	96.5	68.6	174.4	166.6	162.0	63.3	63.3
TS23	123.3	98.7	168.2	165.6	62.6	–174.3	62.6
3A	136.6	110.3	162.8	164.7	164.9	–164.9	58.9
3B	90.8	110.9	163.1	55.7	149.8	–140.4	113.5
B3LYP (**WT_Mn**)							
1B	108.2	74.1	141.6	161.9	67.3	161.8	51.3
TS12	105.5	75.2	152.3	163.5	68.9	168.2	54.5
2A	105.1	75.5	156.3	164.0	69.8	170.4	54.8
TS22	98.4	69.8	173.3	165.7	68.4	164.1	63.2
2B	96.8	69.6	173.0	165.8	69.6	163.7	62.3
TS23	124.1	100.8	169.3	165.7	88.8	–175.1	61.4
3A	134.1	111.3	163.2	163.3	92.4	–160.6	61.6
3B	93.4	111.6	165.1	153.2	57.6	–146.5	150.5

Table S6. Selected geometry parameters, valence (φ) and torsion angles (ϕ) (in degrees) of the optimized transition states and intermediates for the wild-type enzyme with the Mg^{2+} ion (**WT_Mg**) calculated at the hybrid DFT-M06-2X:OPLS2005 and DFT-B3LYP:OPLS2005 levels. For atom numbering see Figure 2.

M06-2X (**WT_Mg**)	φ($O1_D$-$C1_D$-$O5_D$)	φ($O2_A$-$C1_D$-$O5_D$)	φ($O2_A$-$H2_A$-$O1_D$)	φ(O_{Tyr220}-H_{Tyr220}-$O1_D$)	φ(O_{Tyr220}-$C1_D$-$O5_D$)	ϕ($P1_D$-$O1_D$-$C1_D$-$O5_D$)	ϕ($O5_A$-$C2_A$-$C1_D$-$O5_D$)
1B	107.6	74.7	139.9	65.6	65.6	162.3	54.9
TS12	105.8	75.4	149.8	161.6	68.2	169.2	56.8
2A	105.1	75.6	152.1	162.4	68.1	170.4	58.0
TS22	96.7	66.1	173.7	163.7	67.4	160.8	63.9
2B	97.1	68.4	174.1	165.4	69.1	161.9	63.9
TS23	123.8	98.6	168.7	165.3	88.6	–176.0	62.0
3A	137.8	110.2	162.8	163.9	95.7	–165.8	92.8
3B	90.9	111.0	164.3	148.4	55.9	–149.4	113.6
B3LYP (**WT_Mg**)							
1B	108.3	74.1	142.0	161.5	67.1	161.9	51.7
TS12	105.9	75.3	152.1	163.0	69.0	168.7	55.0
2A	105.9	75.6	155.3	163.2	69.9	170.1	55.2
TS22	98.7	69.3	172.9	165.3	68.6	163.5	63.3
2B	97.8	70.1	172.6	165.7	70.1	163.2	62.8
TS23	124.9	100.6	169.7	165,8	89.3	–176.1	61.1
3A	135.2	111.1	163.2	164.7	92.8	–164.0	60.9
3B	94.8	111.6	164.6	153.6	58.6	–146.7	111.2

Table S7. Selected geometry parameters, valence (φ) and torsion angles (ϕ) (in degrees) of the optimized transition states and intermediates for the wild-type enzyme with the Zn^{2+} ion (**WT_Zn**) calculated at the hybrid DFT-M06-2X:OPLS2005 and DFT-B3LYP:OPLS2005 levels. For atom numbering see Figure 2.

M06-2X (**WT_Zn**)	φ($O1_D$-$C1_D$-$O5_D$)	φ($O2_A$-$C1_D$-$O5_D$)	φ($O2_A$-$H2_A$-$O1_D$)	φ(O_{Tyr220}-H_{Tyr220}-$O1_D$)	φ(O_{Tyr220}-$C1_D$-$O5_D$)	ϕ($P1_D$-$O1_D$-$C1_D$-$O5_D$)	ϕ($O5_A$-$C2_A$-$C1_D$-$O5_D$)
1B	107.6	74.2	139.0	158.0	65.9	161.8	54.7
TS12	105.5	75.5	149.8	161.7	68.1	169.0	56.8
2A	104.9	75.7	152.4	162.5	68.0	170.4	58.0
TS22	96.4	66.2	174.0	164.1	67.3	160.7	63.9
2B	96.9	68.6	174.0	166.1	69.5	161.8	63.4
TS23	123.7	98.9	168.4	165.3	88.7	–175.8	61.9
3A	137.2	110.2	162.8	164.1	95.2	–165.2	58.8
3B	91.0	111.0	165.2	149.3	56.1	–148.9	112.8
B3LYP (**WT_Zn**)							
1B	108.3	73.7	140.6	160.5	67.3	161.7	51.5
TS12	106.1	76.6	152.2	162.3	58.5	169.0	55.8
2A	105.9	75.9	155.3	163.1	70.0	170.5	54.8
TS22	99.6	70.1	172.9	164.9	69.0	164.6	62.9
2B	98.0	70.3	172.2	165.5	70.6	163.2	62.1
TS23	124.7	100.3	168.7	165.6	89.4	–175.8	61.4
3A	134.8	111.3	163.1	163.7	92.7	–161.6	61.3
3B	93.9	111.6	166.8	153.4	58.2	–149.1	110.9

Table S8. Selected geometry parameters, valence (φ) and torsion angles (ϕ) (in degrees) of the optimized transition states and intermediates for the wild-type enzyme with the Ca^{2+} ion (**WT_Ca**) calculated at the hybrid DFT-M06-2X:OPLS2005 and DFT-B3LYP:OPLS2005 levels. For atom numbering see Figure 2.

M06-2X (**WT_Ca**)	φ($O1_D$-$C1_D$-$O5_D$)	φ($O2_A$-$C1_D$-$O5_D$)	φ($O2_A$-$H2_A$-$O1_D$)	φ(O_{Tyr220}-H_{Tyr220}-$O1_D$)	φ(O_{Tyr220}-$C1_D$-$O5_D$)	ϕ($P1_D$-$O1_D$-$C1_D$-$O5_D$)	ϕ($O5_A$-$C2_A$-$C1_D$-$O5_D$)
1B	107.6	74.8	140.7	160.5	66.2	160.4	53.4
TS12	140.7	75.7	150.1	163.6	67.5	168.4	56.2
2A	103.1	75.8	155.8	164.7	66.8	170.4	58.5
TS22	95.0	66.4	175.0	166.0	64.4	161.1	63.7
2B	94.5	68.3	173.6	168.8	68.0	162.9	63.3
TS23	122.0	99.0	167.2	166.3	87.9	–175.7	61.8
3A	134.2	110.4	162.6	167.6	92.8	–165.7	59.1
3B	89.9	111.0	164.0	155.0	55.0	–145.7	111.4
B3LYP (**WT_Ca**)							
1B	108.1	77.3	142.2	163.1	67.3	159.5	50.8
TS12	104.1	75.6	155.6	164.7	69.3	168.5	54.9
2A	103.3	75.6	158.0	165.5	68.6	169.9	55.4
TS22	95.7	68.5	173.8	167.5	66.7	163.1	63.5
2B	93.5	68.1	174.7	168.4	67.3	164.4	63.0
TS23	122.6	100.5	167.7	166.8	88.2	**–**175.8	61.0
3A	131.0	111.7	164.7	166.3	90.1	–162.1	62.7
3B	94.7	111.5	163.3	161.3	58.6	**–**141.3	107.6

Table S9. Conformations of the mannose ring of the donor substrate according to the Cremer-Pople parameters and ring puckering geometrical parameters (φ, θ, Q) calculated for the DFT-M06-2X:OPLS2005 and DFT-B3LYP:OPLS2005 optimized transition states and intermediates of the wild-type enzyme with the Mn^{2+}, Mg^{2+}, Zn^{2+} and Ca^{2+} ions (**WT_Mn**, **WT_Mg**, **WT_Zn** and **WT_Ca**).

M06-2X **(WT_Mn)**	GDP^{2-}-Man[a]	φ	θ	Q	M06-2X **(WT_Mg)**	GDP^{2-}-Man[a]	φ	θ	Q
1A	$^4C_1$	13.9	7.4	0.531					
1B	$^4H_3$	220.0	34.5	0.554	**1B**	$^4H_3$	217.8	33.7	0.545
TS12	$^4H_3/^4E$	226.2	42.1	0.539	**TS12**	$^4H_3/^4E$	225.9	42.3	0.538
2A	$^4E/^4H_3$	228.0	45.2	0.541	**2A**	$^4E/^4H_3$	227.7	44.5	0.541
TS22	^4E	250.2	56.2	0.518	**TS22**	^4E	250.4	56.0	0.513
2B	$^4H_5$	263.9	65.9	0.555	**2B**	$^4H_5$	261.2	64.0	0.544
TS23	$^4H_5$	262.2	44.2	0.550	**TS23**	$^4H_5$	263.0	44.3	0.550
3A	$^4H_5/^4C_1$	269.9	21.7	0.557	**3A**	$^4H_5/^4C_1$	271.5	22.1	0.556
3B	$^4C_1$	230.6	9.8	0.565	**3B**	$^4C_1$	230.6	9.6	0.562
B3LYP **(WT_Mn)**					B3LYP **(WT_Mg)**				
1B	$^4H_3$	223.1	30.5	0.539		$^4H_3$	222.2	31.0	0.540
TS12	$^4E/^4H_3$	228.1	40.2	0.535		$^4E/^4H_3$	228.0	41.0	0.534
2A	$^4E/^4H_3$	232.1	42.5	0.532		$^4E/^4H_3$	231.4	42.3	0.532
TS22	^4E	249.8	54.6	0.513		^4E	251.1	55.0	0.512
2B	$^4H_5$	264.4	65.8	0.560		$^4H_5$	264.8	65.8	0.559
TS23	$^4H_5$	260.4	41.5	0.544		$^4H_5$	262.2	41.4	0.540
3A	$^4H_5/^4C_1$	262.0	23.0	0.550		$^4H_5/^4C_1$	265.3	23.2	0.548
3B	$^4C_1$	238.4	9.1	0.548		$^4C_1$	241.4	9.0	0.545

Table S10. Total electronic energies ($E_{QM:MM}$) for the optimized transition states and intermediates for the wild-type enzyme with the Mn^{2+} (**WT_Mn**), Mg^{2+} (**WT_Mg**), Zn^{2+} (**WT_Zn**) and Ca^{2+}(**WT_Ca**) ions calculated at the hybrid DFT-M06-2X:OPLS2005 and DFT-B3LYP:OPLS2005 levels (in a.u.).

M06-2X ($E_{QM:MM}$)	**WT_Mn**	**WT_Mg**	**WT_Zn**	**WT_Ca**
1A	–4710.268781			
1B	–4710.296436	–4806.465982	–4671.777614	–4642.928608
TS12	–4710.282371	–4806.452012	–4671.762321	–4642.913570
2A	–4710.283673	–4806.452811	–4671.763521	–4642.917752
TS22	–4710.271158	–4806.441140	–4671.751431	–4642.903592
2B	–4710.272946	–4806.442498	–4671.753753	–4642.906163
TS23	–4710.263175	–4806.430565	–4671.741227	–4642.897201
3A	–4710.279472	–4806.445859	–4671.758491	–4642.920181
3B	–4710.293959	–4806.459451	–4671.773593	–4642.933570
B3LYP ($E_{QM:MM}$)				
1B	–4711.865422	–4808.075535	–4673.498295	–4644.563556
TS12	–4711.860814	–4808.071746	–4673.492995	–4644.560491
2A	–4711.865191	–4808.075358	–4673.497024	–4644.564842
TS22	–4711.850316	–4808.060581	–4673.483568	–4644.548910
2B	–4711.852533	–4808.063029	–4673.485243	–4644.553582
TS23	–4711.836150	–4808.047420	–4673.461950	–4644.538030
3A	–4711.846962	–4808.053611	–4673.477521	–4644.558315
3B	–4711.854194	–4808.064638	–4673.486160	–4644.563753

Table 1. Calculated pK_a values for selected ionizable amino acid residues in the active site of Kre2p, which are in direct contact with either the Mn^{2+} ion, GDP-Man^{2-} or Met-Man, for six enzyme states.

Residue	Interacted with	E [a]	E/Mn^{2+} [b]	E/Mn^{2+}/ GDP^{2-}-Man [c]	E/Mn^{2+}/GDP^{2-} -Man/ Met-Man [d]	E/Mn^{2+}/ GDP^{3-}/ Man^{+}/ Met-Man [e]	E/Mn^{2+}/ $GDPH^{2-}$/ Met-$(Man)_2$ [f]
Tyr220	GDP^{2-}-Man /Met-Man	14.0	13.5	20.1	19.2	17.4	17.8
Tyr214	GDP^{2-}-Man	10.2	8.6	14.0	14.1	18.8	16.6
Arg130	GDP^{2-}-Man	11.9	14.4	14.6	14.5	12.4	12.0
Arg245	GDP^{2-}-Man	12.7	12.8	11.3	11.2	11.6	11.8
Asp361	GDP^{2-}-Man	2.6	2.6	1.3	1.4	0.8	2.2
Asp161	GDP^{2-}-Man	1.5	3.9	–2.8	–2.8	–3.5	–3.6
His388	Mn^{2+}	2.7	1.2	4.0	3.9	2.6	3.2
Glu247	Mn^{2+}	4.9	–3.0	1.8	1.9	2.4	2.5
Arg358	Met-Man	15.0	14.8	14.5	14.1	13.2	12.9
Glu279	GDP^{2-}-Man /Met-Man	4.0	3.9	2.5	2.2	3.5	3.2
His323	Met-Man	2.1	2.0	0.9	0.6	–0.1	–0.2
Tyr391	Met-Man	10.2	10.0	10.0	10.1	11.1	11.1
Tyr280	Met-Man	9.9	9.8	9.8	9.8	15.7	13.9

[a] (E) - an apoenzyme with an empty active site (a geometry from PDB ID: 1S4N); [b] (E/Mn^{2+}) - manganese ion bound to the enzyme (a geometry from PDB ID: 1S4O); [c] [E/Mn^{2+}/GDP^{2-}-Man(donor)] - a binary complex of the enzyme with Mn^{2+} and GDP^{2-}-Man; [d] [E/Mn^{2+}/GDP^{2-}-Man(donor)/Met-Man(acceptor)] - the Michaelis complex **1B**; [e] [E/Mn^{2+}/GDP^{3-}/Man^{+}/Met-Man] - the oxocarbenium ion intermediate **2B**; [f] [E/Mn^{2+}/$GDPH^{2-}$/Met-$(Man)_2$] - the product **3A**, all structures were optimized at the QM/MM level based on a crystal structure geometry (PDB ID: 1S4P).

Computational details

pK_a calculations

The protonation states of ionizable amino acid residues were predicted at the empirical level using the PROPKA v. 2.0 program[1-2] considering an enzyme pH optimum of 6.6. The pK_a values were calculated for six enzyme structures (Table S11): the apoenzyme, the complexes enzyme/Mn^{2+}, enzyme/Mn^{2+}/GDP^{2-}-Man (donor) and enzyme/Mn^{2+}/GDP^{2-}-Man (donor)/Met-Man(acceptor) in the three chemical states, in the Michaelis complex (**1B**), the oxocarbenium ion intermediate (**2B**) and product (**3A**). The pK_a values were calculated for geometries obtained from the PDB structures [PDB ID: 1S4N (apoenzyme) and PDB ID: 1S4O (enzyme/Mn^{2+})][3] and for optimized geometries from the QM/MM calculations (enzyme/Mn^{2+}/donor, **1B**, **2B** and **3A**).

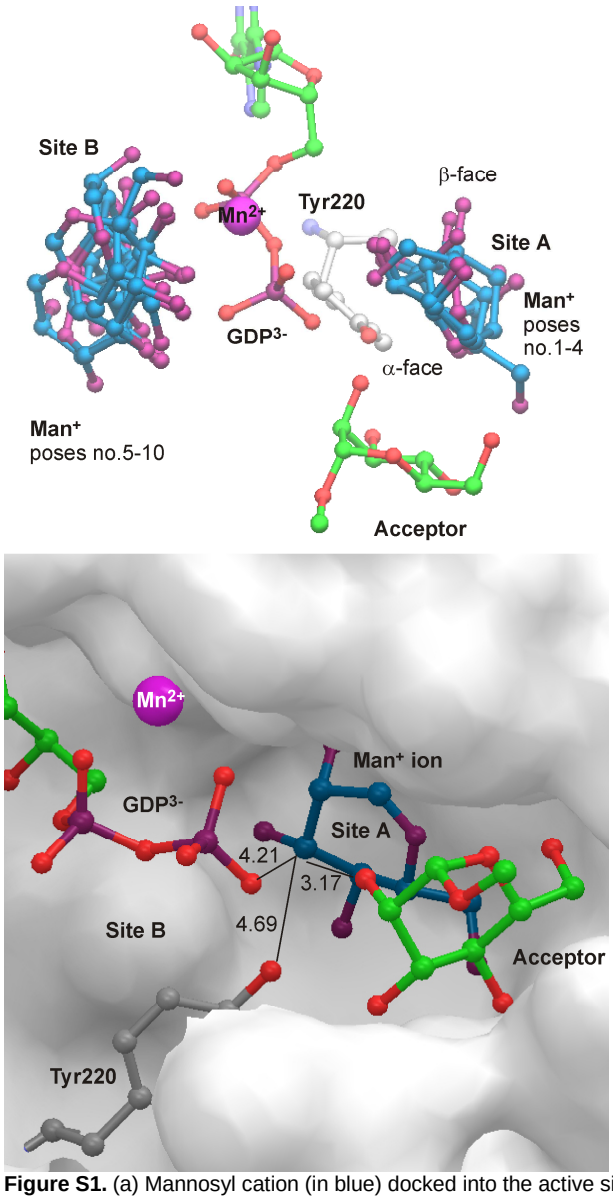

Figure S1. (a) Mannosyl cation (in blue) docked into the active site of Kre2p (10 poses with the best docking score) bound to the A and B binding sites (see also Table S1). (b) The docked pose no A1 [ϕ($P1_D$-$O1_D$-$C1_D$-$O5_D$) = 168.5°] with selected geometry parameters (distances in Å).

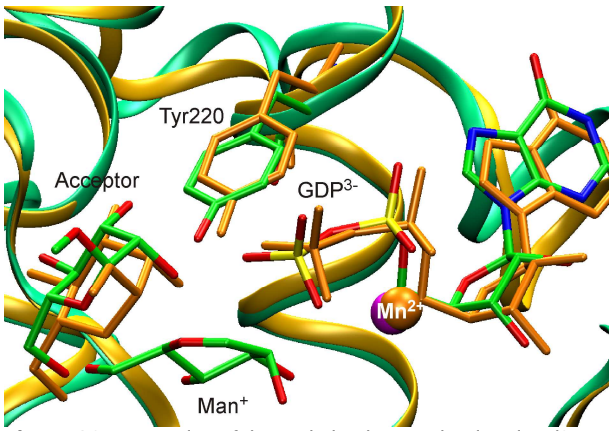

Figure S2. An overlay of the optimized oxocarbenium ion (**2B**, **WT_Mn**, in green) with the crystal structure (in orange) of Kre2p (PDB ID: 1S4P).

Docking

The missing α-D-mannosyl moiety of the donor substrate was docked as a mannosyl cation (Man^+) into a ternary complex of Kre2p (PDB ID: 1S4P)[3] employing the GLIDE program[4-5] of the Schrödinger package. The structure of Man^+ was prepared with the MAESTRO viewer[6] and optimized in the gas phase at the density functional theory (DFT) level (M06-2X/LACVP**+, for more details see the next section)[7-9] using the Jaguar program[10] of the Schrödinger package. All crystallographic water molecules were deleted for the docking procedure. Glide uses Schrödinger´s discrete version of the ChemScore empirical function.[11] For the docking calculations, default parameters were used. The receptor box for the docking conformational search was centered at the diphosphate group of GDP^{3-} bound in Kre2p, with a size of 30×30×30 Å using partial atomic charges for the receptor from the OPLS2005 force field.[12] The grid maps were created with no Van der Waals radius and charge scaling for the atoms of the protein. Flexible docking in standard precision was used with no sampling of the ring conformations for the docked ligand. The Man^+ ligand was docked into the receptor with atomic partial charges calculated at the M06-2X/LACVP+** level.[7-9] The potential for nonpolar parts of Man^+ was softened by scaling the Van der Waals radii by a factor of 0.8 for atoms with partial atomic charges less than the specified cutoff of 0.15. In total, 5000 poses were kept per ligand for the initial docking stage with a scoring window of 100 kcal mol^{-1} for keeping initial poses. The best 400 poses were kept per ligand for energy minimization. The ligand poses with RMS deviations less than 0.5 Å and maximum atomic displacement less than 1.3 Å were discarded as duplicates. The post-docking minimization for the 20 poses with the best docking scores was performed, and optimized structures were saved for later analysis.

In addition, we also docked into the active site a product (Met-Man-Man) and a whole donor substrate, GDP^{2-}-Man (in absence as well as in the presence of the bound terminal moiety of the acceptor substrate), to analyze possible conformations of the donor substrate upon binding to the active site, and possible conformations of the product after the catalytic reaction. Based on these calculations, starting structures for the Michaelis complex (**1A**) and product (**3B**) were built.

Results

pK_a calculations. Both Tyr214 and Tyr220 are highly conserved across the family except in Ktr6p. The role of Tyr220 in the substrate binding and catalysis is supported by mutagenesis data.[3] A kinetic analysis of the Y220F mutant revealed that the k_{cat} was only 0.035% that of the wild-type enzyme.[3] It is not clear whether Tyr220 could play the role of catalytic nucleophile or its role is in stabilizing electron deficient oxocarbenium ion transition state (OCI-TS) or oxocarbenium ion intermediate (OCII). Its position on the β-face of the anomeric reaction center was not confirmed by crystallographic measurements due to the missing coordinates of the mannose ring of GDP^{2-}-Man bound at the active site of Kre2p.[3]

pK_a values for all ionizable amino acid residues of the catalytic domain of Kre2p were calculated with three main aims: (i) to build a 3-D enzyme model with correctly assigned protonation states for QM/MM calculations; (ii) to investigate whether Tyr220, a candidate for the catalytic nucleophile, prefers *in vivo* the ionized phenolate state that is favorable for the nucleophilic substitution reaction with a substrate; and (iii) to analyze whether the protonation states of the ionizable amino acid residues in the active site change during the catalytic cycle of Kre2p, i.e. whether they are in the same protonation state for an apoenzyme, Michaelis complex, intermediates and products. It should be noted that incorrect assigning of protonation states or ignoring protonation interconversions of the active-site ionizable residues could lead not only to misleading thermochemical kinetics predictions but also to an incorrect mechanistic proposal of the catalytic mechanism.

As it is compiled in Table 1, ionizable amino acid residues, which directly interact with either substrates or a metal ion cofactor, prefer standard ionization states in all chemical states of the Kre2p cycle, i.e. Asp and Glu residues prefer anionic states: His, Tyr and Cys residues neutral ones; and Arg residues cationic ones. In the pK_a analysis we focused on Tyr220 as a possible candidate for the catalytic nucleophile. Its pK_a value was predicted to be 14.0 pK_a units in the apoenzyme. After binding metal ion cofactor, donor and acceptor substrates to the active site its value further increased (Table 1). The high values of 13.5-20.1 for all calculated chemical states indicate that Tyr220 is extremely weak acid and strongly prefers the protonated phenol form in *in vivo* pH. The high pK_a value also influences its nucleophilic properties, thus Tyr220 would participate in catalysis as a very weak nucleophile unwilling to release a proton during the catalytic reaction.

Docking. Because of the missing coordinates of the mannose moiety of GDP^{2-}-Man bound in the active site of a crystal structure of Kre2p, we docked a mannosyl cation to the active site in the presence of GDP^{3-}, the Mn^{2+} ion cofactor and Met-Man acceptor. The Glide program predicted two distinct binding sites for Man^{+} (we called them the sites A and B, Figure 4). The first four energetically favorable poses were placed in the binding site A (Table S1 in Supporting Information). The remaining 16 poses occupied the B site from which the enzymatic reaction would lead to the formation of the stereochemically unwanted β-1,2 glycosidic linkage. Consequently, these poses were excluded from the structural analysis and will not be discussed further. The binding site A is situated in the area where Man^{+} is in contact (≤ 3 Å) with the diphosphate group of GDP^{3-}, Met-Man, Tyr220, Met223, Glu247, Arg245, Asn327, Ser326, Pro363, Ala362, Asp361, Gly360 and Glu279. At this binding site the bound acceptor substrate, Met-Man, is positioned on the α-face of the $C1_D$ reaction center of docked Man^{+} (the poses no. A1, A3 and A4); thus, the position of Man^{+} in the binding site A is perfectly fitted for the stereoselective formation of the α-1,2 glycosidic linkage in the product. In the pose with the best docking score (no. A1), the $C1_D$ reaction center of Man^{+} interacts on the α-face with the $O1_D$ phosphate oxygen of GDP^{3-}, the $O2_A$ hydroxyl oxygen of Met-Man and the O_{Y220} hydroxyl oxygen of Tyr220 [$d(O1_D\text{-}C1_D)$ = 4.21 Å, $d(C1_D\text{-}O2_A)$ = 3.17 Å and $d(C1_D\text{-}O_{Y220})$ = 4.69 Å, Table S1 of Supporting Information] and is characterized by a dihedral angle between the mannose ring of the oxocarbenium ion and the phosphate group of GDP^{3-}, $\phi(P1_D\text{-}O1_D\text{-}C1_D\text{-}O5_D)$ = 168.5°. The pose no. A2 would not fit the stereochemistry of the enzymatic reaction because the nucleophilic 2-OH group of the acceptor is situated on the β-face of Man^{+} in this case. The other binding poses (no. A3 and A4) predicted for the site A show the mannosyl ring in less favorable orientations for the enzymatic reaction [$d(O1_D\text{-}C1_D)$ = 5.12 and 5.11 Å; $\phi(P1_D\text{-}O1_D\text{-}C1_D\text{-}O5_D)$ = –148.4° and –151.8° for poses no.A3 and A4] as well as less favorable docking score energy (Table S1 of Supporting Information). Therefore, only the first docked pose of Man^{+} was considered for the following QM/MM calculations of the enzymatic reaction. The optimization of the pose no.A1 at the QM/MM level resulted in an oxocarbenium ion, which was verified by vibrational frequency calculations as a minimum. In PES QM/MM calculations along the $C1_D\text{-}O1_D$ α-glycosidic bond of GDP^{2-}-Man, it resulted in a Michaelis complex with the *(+ap)* conformation of the mannose ring related to the diphosphate group of the GDP^{2-}-Man donor substrate [$\phi(P1_D\text{-}O1_D\text{-}C1_D\text{-}O5_D)$ = 163.1°]. We will discuss in more detail the structural and energetic analysis of the oxocarbenium ion intermediate and Michaelis complex in the sections.

In all Man^{+} poses bound at the site A, the Tyr220 residue is always situated on the α-face of the $C1_D$ reaction center. The speculation that Tyr220 could play the role of the catalytic nucleophile,[3] based on a comparison of positions of bound donor substrates in crystal structures of Kre2p and the retaining GT LgtC,[13] is not supported by the calculations. The nucleophilic substitution reaction of Tyr220, with either GDP^{2-}-Man

or oxocarbenium ion intermediate, would not result in a feasible inversion of the anomeric center in the covalent substrate-enzyme intermediate. Subsequently, an attack of the acceptor in next reaction step would occur from the β-face giving the wrong stereo configuration of the anomeric center in the product. As discussed in the previous section, the pK_a calculations do not support the idea about the nucleophilic role of Tyr220 since they disfavor the existence of the nucleophilic phenolate form of Tyr220 during the enzymatic reaction.

References:

1. D. C. Bas, D. M. Rogers and J. H. Jensen, *Proteins*, 2008, **73**, 765-783.

2. H. Li, A. D. Robertson and J. H. Jensen, *Proteins*, 2005, **61**, 704-721.

3. Y. D. Lobsanov, P. A. Romero, B. Sleno, B. Yu, P. Yip, A. Herscovics and P. L. Howell, *J. Biol. Chem.*, 2004, **279**, 17921-17931.

4. Glide, version 5.7, Schrödinger, LLC: New York, NY, 2011.

5. R. A. Friesner, J. L. Banks, R. B. Murphy, T. A. Halgren, J. J. Klicic, D. T. Mainz, M. P. Repasky, E. H. Knoll, M. Shelley, J. K. Perry, D. E. Shaw, P. Francis and P. S. Shenkin, *J. Med. Chem.*, 2004, **47**, 1739-1749.

6. Maestro, version 9.2; Schrödinger, LLC: New York, NY, 2011.

7. Y. Zhao and D. G. Truhlar, *Theor. Chem. Acc.*, 2008, **120**, 215-241.

8. W. R. Wadt and P. J. Hay, *J. Chem. Phys.*, 1985, **82**, 284-298.

9. P. J. Hay and W. R. Wadt, *J. Chem. Phys.*, 1985, **82**, 270-283.

10. Jaguar, version 7.8, Schrödinger, LLC: New York, NY, 2011 New York, NY, 7.8 edn., 2011.

11. M. D. Eldridge, C. W. Murray, T. R. Auton, G. V. Paolini and R. P. Mee, *J. Comput.-Aided Mol. Des.*, 1997, **11**, 425-445.

12. G. A. Kaminski, R. A. Friesner, J. Tirado-Rives and W. L. Jorgensen, *J. Phys. Chem. B*, 2001, **105**, 6474-6487.

13. K. Persson, H. D. Ly, M. Dieckelmann, W. W. Wakarchuk, S. G. Withers and N. C. J. Strynadka, *Nat. Struct. Biol.*, 2001, **8**, 166-175.